ACS Photonics

Letter

pubs.acs.org/journal/apchd5

Electrochemical Tuning of the Dielectric Function of Au Nanoparticles

Ana M. Brown, Matthew T. Sheldon, and Harry A. Atwater*

Thomas J. Watson Laboratories of Applied Physics, California Institute of Technology, MC 128-95, Pasadena, California 91125, United States

Supporting Information

ABSTRACT: The tunable dielectric response of Au nanoparticles under electrochemical bias can be interpreted in terms of changes in the surface charge density, surface damping, and the near-surface volume fraction of the nanoparticles that experience a modified dielectric function, as well as changes in the index of refraction of the surrounding electrolyte medium. Using experimental bias-dependent extinction measurements, we derive a potential-dependent dielectric function for Au nanoparticles that accounts for changes in the physical properties contributing to the optical extinction.

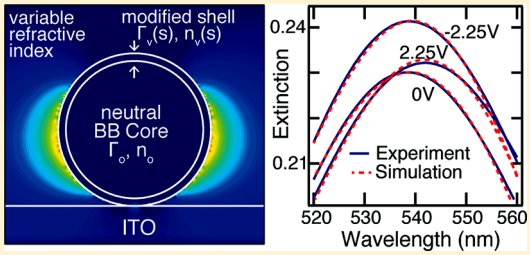

KEYWORDS: *plasmonics, electro-optical tuning, electrochemistry, surface damping, localized surface plasmon resonance, FDTD simulations*

The plasmonic response of metal nanoparticles has generated great scientific interest, motivating both fundamental investigations and exploration of a variety of applications, such as photovoltaic cells,[1] photocatalytic fuel cells,[2,3] surface enhanced Raman spectroscopy (SERS),[4−7] cell labeling, and molecular sensing.[6,8−12] These complex environments modify the plasmonic behavior in several ways due to the material dynamic response under electrochemical potential changes, by the equilibration of the particle with the surrounding Fermi-level offset, and the effects of chemical reactivity, solvent polarizability, and interface damping.[13−20] In order to achieve precise manipulation of the properties of metallic resonators in tunable plasmonic systems, we are fundamentally interested in how changes of charge density and the properties of the surrounding environment, such as refractive index and electronic surface states, affect the plasmonic absorption. The Drude model can be used as a first approximation to predict how a change in charge density through an applied bias tunes the plasmonic resonance.[2,10,12,21] However, it is well-known that plasmon resonances are dependent on their environment,[1,4,6,7,16,22,23] and a simple Drude model omits a description of property changes other than a uniform change in charge density. The Drude model does not take into account other effects that happen in parallel with changes in charge density in a real system, such as changes in electronic surface states due to chemical interactions with the surrounding medium and the resultant changes in damping and index of refraction (e.g., adsorbates, oxidation, electric double layer).[6,8,10−12,16,20,24] Furthermore, using a Drude model to represent a uniform change in charge density in a plasmonic structure does not account for the excess charge residing at the conductor surface. Thus, in order to predict optoelectronic behavior of plasmonic systems, we desire a model that will account not only for changes in charge density, but also for changes in damping, index of refraction, and penetration depth of surface charge and damping. This will allow us to assess the relative spectral contributions of each effect, and how they act in concert in an electrically tuned plasmonic system. Better quantification of the various contributions that shape plasmonic resonances is crucial for current research in tunable plasmonics, and more broadly, for any system in which plasmonic elements will be used an a non-neutral state, for example, as catalysts or electrical contacts.

Previous experiments have shown that externally biased Au nanoparticles (AuNPs) are not adequately described by the Drude model.[10,12,16,21,22,25,26] A potential-dependent modified dielectric function and T-matrix-based fitting routine has been proposed to analyze interface damping and uniform charging effects for Au nanorods in an electrochemical cell.[21] This work provided a systematic model for bias-dependent extinction, but did not explicitly address index changes in the surrounding media or nonuniform distribution of charge at the particle surface.[21,27] Separately, the effects of various surface layers on the dielectric response of Au nanoparticles in an electrochemical cell were investigated, in comparison with modeling that relied on analytical Mie Theory, though analysis of broadening effects and the role of the refractive index of the substrate were not considered.[10,27,28] These researchers found evidence of increased damping at a positive applied bias, which they attributed to a lossy layer at the particle surface. Previous research has not analyzed the effects of changes in the surrounding dielectric environment, changes in damping, and concentration of excess charge at the particle surface all

Received: September 30, 2014
Published: March 10, 2015

DOI: 10.1021/ph500358q
ACS Photonics 2015, 2, 459−464

occurring in unison. In this Letter, we investigate mechanisms for bias-dependent optical extinction of Au nanoparticles, using full wave electromagnetic simulations in conjunction with experimental optical spectra to characterize the response of arrays of colloidal Au nanoparticles immobilized on indium tin oxide (ITO) substrates in an electrochemical cell. Through this combined simulation and experimental approach, we account for the influence of refractive index due to the substrate, index changes in the near-surface environment of the nanoparticle, and a variable-thickness shell of modified damping and charge density at the surface of the gold nanoparticle (AuNP). We compare the simulations with experimental results to quantitatively analyze the contributions from these effects.

METHODS

In our experiment, the spectra of an ensemble of 30 nm radius Au colloids in an electrochemical cell were recorded as a function of applied bias. The applied bias was swept from 0 to 2.25 V then to −2.25 V and back to 0 V in 0.25 V steps. To prepare the capacitive electrochemical cell, ITO coated glass substrates (SPI brand, 30−60 Ω, 06430) were used as the top and bottom electrodes (Figure 1). Au particles were deposited

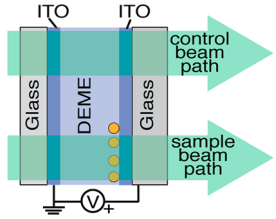

Figure 1. Geometry of electrochemical cell with 30 nm radius AuNPs on the bottom electrode. The top electrode is grounded, and potentials are applied to the bottom electrode. An optical beam passes through the cell for spectral measurements.

on one-half of the bottom substrate, thereby reserving half of the bottom electrode for use as a control in the normalization of optical spectra; this allowed us to carefully control for a possible optical response from the ITO substrate as a function of applied bias (see the Supporting Information for electrochemical cell fabrication details). Diethylmethyl(2-methoxyethyl)ammonium bis(trifluoromethylsulfonyl)imide (DEME) was used as the electrolyte. The top electrode was grounded and potentials were applied to the bottom electrode using a DC voltage source (Tektronix PS282). The extinction spectra of an array of AuNPs in the electrochemical cell were obtained using a spectral response and lock-in amplifier technique (see Supporting Information for detailed experimental procedures). Approximately 20 min elapsed between each voltage step and the corresponding spectral measurement.

RESULTS AND DISCUSSION

Figure 2a shows the extinction spectra for AuNPs in the electrochemical cell at selected values of applied bias, which were smoothed with a Savitsky-Golay filter. A red-shift of the peak is observed at positive applied bias and a blue-shift and increase in peak height is observed under negative applied bias. The shift of the peak is more evident in the extinction change spectra (Figure 2b) where a red shift is manifest as a positive change in extinction to the red of the peak and a negative change in extinction to the blue of the peak and vice versa for a blue-shift. Figure 3 shows the change of the spectral properties

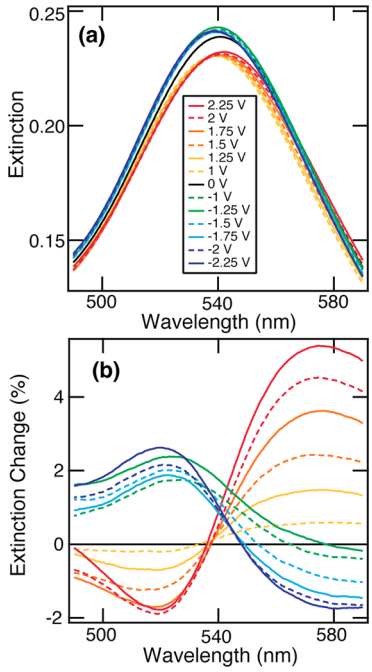

Figure 2. (a) Extinction vs wavelength at selected applied potentials as indicated by line color. (b) Extinction change vs wavelength at the same applied potentials in (a).

as a function of applied bias. Over the range of applied potentials, the wavelength of peak extinction shifted by 3 nm and the full width half-maximum of the peak varied by 4 nm (Figure 3a,c). The total peak extinction change was 7% of the initial 0 V peak extinction (Figure 3b). The hysteresis in the experimental results indicates some nonreversible process and that this electrochemical system does not exhibit ideal reversible charging. Additionally, we find that at negative applied potentials, the peak height increases. This is in contrast to what we would expect based on the Drude model and Mie theory,[22,25,28] which predict a peak height change that decreases monotonically as a function of increasing electron density. This suggests that, at the very least, there is significant damping in the experimental system at positive potentials that is not captured by a Drude and Mie theory model.

Three-dimensional full wave electromagnetic simulations were performed using finite difference time domain methods to model and analyze the experimental system. The simulation geometry consisted of a 30 nm radius Au nanosphere on an ITO substrate and in a surrounding medium with uniform index of refraction (Figure 4). The ITO substrate was defined by the real and imaginary part of the complex index of refraction, measured with ellipsometry. The AuNP was simulated as a core defined by the Brendel and Bormann (BB)[6,7,27,29] dielectric function with the additional feature of a variable-thickness shell with a modified dielectric function. The BB model uses a superposition of an infinite number of oscillators (termed a BB oscillator) to replace the single Lorentz oscillator used in the Lorentz−Drude model.[12,27,28,30] The BB dielectric function is defined as

$$\varepsilon_{BB}(\omega) = 1 - \frac{{\omega_p}^2}{\omega(\omega - i\Gamma_o)} + \sum_{j=1}^{k} \chi_j(\omega)$$

DOI: 10.1021/ph500358q
ACS Photonics 2015, 2, 459−464

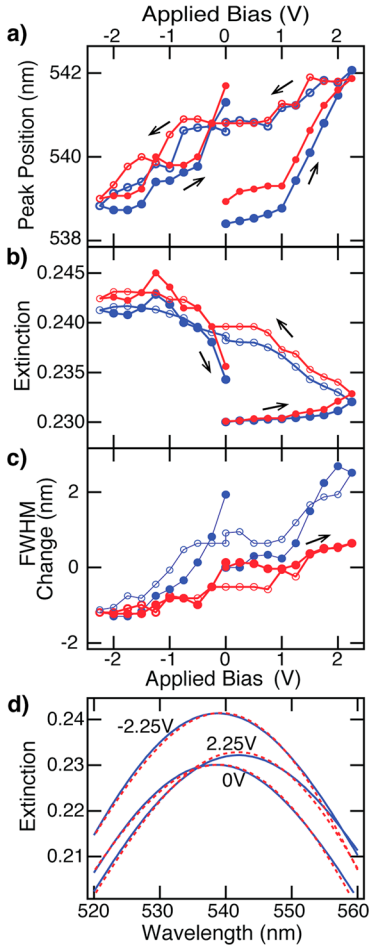

Figure 3. Experimental results are displayed in blue; simulation results are displayed in red. (a) Peak position, (b) peak extinction, and (c) full with half max change relative to the first 0 V applied bias point vs applied bias. For a−c, the markers for the applied bias points for the middle portion of the cycle, from 2 V to −2.25 V in −0.25 V steps are hollow. (d) Experimental extinction spectra at 0, +2.25, and −2.25 V and their best-fit simulated spectra.

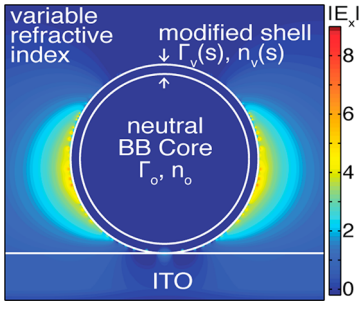

Figure 4. Full wave FDTD simulation, *x*-component of the electric field in a *y*-normal cross-section. The 30 nm radius particle is modeled by a neutral core defined by the BB model and a shell with a modified dielectric that allows for variations in damping and charge density at the surface. The substrate is defined by measured n&k data and the electrolyte is modeled as a uniform dielectric above the substrate. The varied simulation parameters are shell charge density, shell damping, shell thickness, and refractive index of the electrolyte.

$$\omega_{\mathrm{p}} = \left(\frac{n_{\mathrm{o}} \times e^2}{\varepsilon_{\mathrm{o}} \times m_{\mathrm{e}}}\right)^{1/2}$$

where Γ_{o} is the damping constant of bulk gold, $\chi_j(\omega)$ is a BB oscillator, ω_{p} is the plasma frequency in the Drude model, n_{o} is the electron density of bulk gold, e is the elementary charge, and m_{e} is the effective electron mass. Six BB oscillators were used in our parametrization. We obtain an analytic function that satisfies the Kramers−Kronig reciprocity relations for real and imaginary components of the dielectric function. This model has been shown to accurately model the optical properties of gold in the wavelength range relevant to this study.[8,28,31−34]

A modified dielectric function at the surface of the particle is used to model changes in the electronic states and population near the surface:

$$\varepsilon_{\mathrm{shell}}(\omega, s) = 1 - \frac{\omega_{\mathrm{p},V}(s)^2}{\omega(\omega - i(\Gamma_{\mathrm{o}} + \Gamma_V(s)))} + \sum_{j=1}^{k} \chi_j(\omega)$$

$$\omega_{\mathrm{p},V}(s) = \left(\frac{n(s) \times e^2}{\varepsilon_{\mathrm{o}} \times m_{\mathrm{e}}}\right)^{1/2}$$

Here, $\omega_{\mathrm{p,V}}(s)$ and $n(s)$ are state (s) dependent variables, where the state describes the applied bias (V) applied to the cell and the microscopic state of the system, and these state-dependent variables have replaced the respective constant values used in the BB model. An additional, state-dependent damping term $\Gamma_V(s)$ has been added to the bulk damping to allow for changes for damping at the particle surface as a function of the state of the system (largely, the applied bias).

The independent parameters that were varied in our analysis are the index of surrounding electrolyte, and Γ_V and $n(s)$ in the shell dielectric function, as well as the thickness of this shell. Additionally, to account for polydispersity in the size of particles (8% coefficient of variation as reported by the supplier), we performed electromagnetic simulations for particles with 28, 30, and 32 nm radii and took a weighted average of the resulting spectra to produce simulated extinction spectra for polydisperse samples for each parameter set (surrounding-index, Γ_V, $n(s)$, and shell-thickness). We performed calculations where each of these parameters was varied independently. For each unique parameter set, a full-wave electromagnetic simulation was performed to simulate the extinction spectra corresponding to that parameter set. This approach allowed us to calculate a set of predicted extinction spectra from the effect of changes in index, interface damping changes, and surface charging occurring in parallel. We began parameter sweeps across large ranges where the values for parameters found in current literature describing damping, surface effects, charging, or electric double layer were well within the sweep limits.[8,10,26,28,31] Next, we performed an iterative process for finding the values of parameters that produced simulated extinction spectra with smallest root-mean-square error (RMSE) in comparison to the Savitsky-Golay smoothed experimental extinction spectra. After each parameter sweep, a new parameter sweep with finer resolution of the parameter space around the parameter values that had produced the lowest error was preformed. Using this iterative process, we determined the parameter values that most closely reproduced the experimental spectra at each applied bias, stopping simulations when an acceptably small parameter step size was reached and the RMSE was below 1% error. The parameters values for these simulations then represented the identifiable physical properties and changes in the system as

DOI: 10.1021/ph500358q
ACS Photonics 2015, 2, 459−464

determined by our model (see Supporting Information for further discussion of simulation methods)

We believe the model described above represents the most comprehensive analysis to date of the microscopic mechanisms that can contribute to bias-dependent optical extinction for metal nanoparticles. We now discuss the physical basis for the observed variation of nanoparticle parameters. Because gold oxide has a larger dielectric constant than the electrolyte solution, oxidation of the AuNP surface will cause changes of the index of refraction at the surface of the metal nanoparticle relative to an unoxidized Au particle.[6−8,29,35] Further, the refractive index of the surrounding medium could also change due to alignment of dipoles in the electrolyte, as in an electric double layer.[12,16,20,24,26,30] Damping may also be modified by an applied bias because of variations of population or depopulation of electronic surface states at the AuNP surface.[8,31−34] For example, an applied bias could facilitate enhanced chemical reactivity and adsorption at the particle surface and electrons may become trapped in empty adsorbate states, causing an increase in damping.[8,35] Alternatively, an increase in electron density due to a negative applied bias could result in electron spill-out from the surface and repulsion of solvent molecules from the AuNP surface.[3,36,37] This could conceivably give rise to a decreased damping due to a decrease in chemical reactivity and trap state occupation at the particle surface. It is also reasonable to assume that the applied bias will alter the total number of electrons in the AuNP and thereby alter the plasma frequency in accordance with the Drude model.[17,18] In the electrostatic limit, mobile charges will rearrange to minimize the electric fields in the bulk of a conducting particle, so we assume that excess electrons or holes reside near the particle surface. Finally, the modified electronic states and electron density at the surface may have a variable penetration depth that depends on the applied bias because of the aforementioned electron spill-out, adsorbate states, and the optical versus the static skin depth of excess charge residing near the surface. We account for changes in the penetration depth of altered electronic states by varying the thickness of the modified dielectric shell in our simulations.

By varying the charging, damping, shell thickness, and electrolyte index independently of one another in our parametric calculations and by computing their net influence on the extinction spectra, we were able to closely model the experimental changes in the extinction as a function of applied bias with full wave electromagnetic simulations. Figure 3 shows a comparison of the spectral properties of the simulated and experimental spectra. We see that the best-fit simulations closely track the peak position, height, and changes in width. Furthermore, in Figure 3d, we show the experimental and best-fit simulated spectra at the extrema of the applied bias range (2.25 and −2.25 V) as well as at the first 0 V applied bias point, with very good agreement between the curves. We note that the absolute fwhm is sensitive to peak broadening due to particle size poly disparity and other ensemble effects[18,26] that are not well captured by our FDTD simulations, though changes of fwhm (Figure 3c) are primarily due to changes in damping and, therefore, are expected to be tracked well by our analysis method. See the Supporting Information for details. From Figure 5a we note that the maximum RMSE of the fits of the simulated and experimental spectra was less than 0.8% of the experimental 0 V peak extinction.

The results from performing simulations to obtain the best-fit simulation for each experimental spectra provides a parameter set for the model that is appropriate at each applied bias step. These results are shown in Figures 5b−e. Our analysis indicates that at the initial 0 V data point, before any external voltage has been applied to the electrochemical cell, at the surface of the particle there is an elevated electron density of 1% compared to neutral bulk Au (Figure 5b). This may be due to Fermi level offsets between the ITO, electrolyte, and AuNPs or due to interactions with the electrolyte at the surface of the particles. Note we do not claim a uniform increase of electron density throughout the particle, but only a 1% increase in the surface shell region of the metal particle. As the applied bias becomes more positive, the electron density decreases, and then increases as the applied bias becomes more negative, as expected; however, there is significant hysteresis that is not consistent with reversible, ideal charging. The overall shell charge density range for the applied potentials used was within

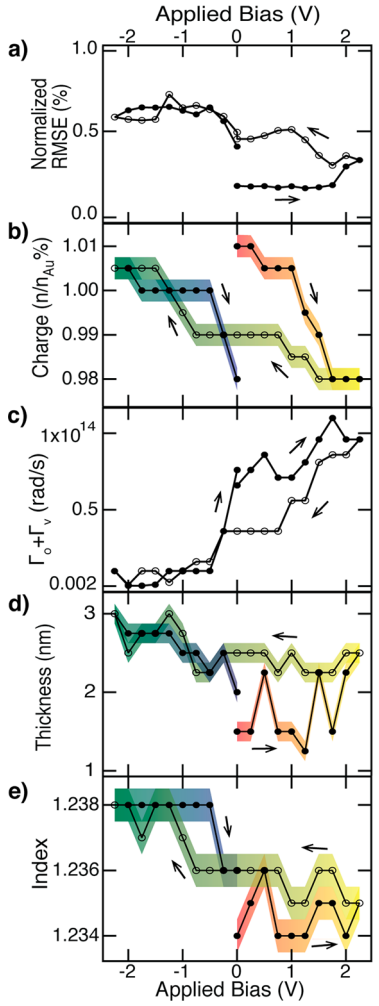

Figure 5. Parameters of the simulations that produced the spectra best-fit to the experimental spectra. (a) Root mean square error of the simulated spectra fit to the experimental spectra, normalized as a percentage of the initial 0 V peak extinction. (b) Charge (electron) density and (c) total damping in the modified-dielectric particle shell vs applied bias. (d) Thickness of the modified-dielectric particle shell vs applied bias. (e) Refractive index of the surrounding medium above the ITO substrate vs applied bias. For parts b−e the height of the colored band represents the error due to the finite step size used in the parameter sweeps. For (c), the step size for Γ is smaller than the thickness of the black line. The color of the band goes from red to blue in time.

DOI: 10.1021/ph500358q
ACS Photonics 2015, 2, 459−464

3% of the neutral charge density. The hysteresis upon charging/discharging is strongest in the first half of the applied bias cycle (from 0 to 2.25 V and back to 0 V). This is a common feature in cyclic voltammetry measurements and may be due to initial chemical reactions or "settling" of the system during this initial application of an electric field.

The results for the damping parameter exhibit an overall trend of increased damping at positive biases and decreased damping at negative biases (Figure 5c). The damping coefficient used in the BB model to best describe neutral, bulk Au metal is $\Gamma_o = 7.596 \times 10^{13}$ rad/s.[20] At the first 0 V data point, we found the damping constant was 1×10^{13} rad/s less than this value, indicating that the damping of plasmons on the AuNPs in this system is less than in bulk gold. Recalling that this data point corresponds to a 1% elevation of electron density in the particle shell, we speculate that the decreased damping could be due to electron spill-out and a resulting interlayer where the solvent is repelled and electron trapping in surface or adsorbate states is decreased, resulting in an electron configuration that experiences less damping than in the bulk. At +2.25 V, we found $\Gamma_V = 3 \times 10^{13}$ rad/s. The increase in damping at positive applied voltages is consistent with prior published work[6,8−10] and may be due to excitation of sp-electrons in adsorbate states at the surface of the particle. Again, at negative voltages, as in the first 0 V case, we found that the damping was lower than for neutral, bulk Au metal (at −2.25 V, $\Gamma_V = -6.6 \times 10^{13}$ rad/s), and we similarly attribute this to decreased reactivity and electron spill-out at the particle surface.

The thickness of the modified-dielectric particle shell of the best-fit simulations is shown as a function of applied bias in Figure 5d. We found that the shell thickness varies between 1 and 3 nm. This thickness is greater than the electrostatic skin depth of bulk metal (i.e., the Fermi screening length is ∼0.3 nm for Au) and less than the optical skin depth of the nanoparticle (∼10 nm), as determined from full wave simulations. Our simulations suggest that the shell thickness increases during the first rise in applied bias and then continues to increase more gradually at negative applied biases. The initial increase in shell thickness may be due to reactivity with the electrolyte as the system "settles" under the initial application of voltage. The electronic structure at the surface changes significantly during this period, enough for the effects on the dielectric constant to penetrate a few nanometers into the surface of the particle. It is also reasonable to suggest that the shell thickness increases at negative applied biases because the associated increase in electron density at the surface might result in the zone with a modified dielectric function protruding deeper into the particle. We believe that the thickness of the metallic shell with a modified dielectric function corresponds to the region of the particle whose electronic structure is modified due to adsorbates, surface states, and an excess or deficit of electrons at the surface.

Finally, Figure 5e shows the results for the index of the surrounding medium as a function of applied bias. We found less than a 1% change in the refractive index of the surrounding medium. There is an overall trend indicating a slight increase in index as the applied bias goes from positive to negative. This small change could be due to a difference in the index of refraction of the cation and anion of the DEME electrolyte and alignment of these dipoles in an electric double layer.[24,26] Significantly, we did not see an increase in the index at positive voltages as would be expected in the case of oxidation of the AuNP surface in to Au_xO_x. We note that the formation of Au halide surface compounds, induced by chemical reaction with impurities in the DEME electrolyte (<1% by supplier assay), for example, is similarly inconsistent with our observations, as Au halides are also expected to exhibit a larger refractive index.

In conclusion, we have shown that by using full wave electromagnetic simulations to model a AuNP with a variable-thickness conducting shell with a modified dielectric function, a variable electrolyte index, and an explicitly modeled ITO substrate, we are able to find good fits to experimental extinction spectra and track changes in the spectra as a function of applied bias. The best-fit simulation spectra correspond to a set of simulation parameters as a function of applied bias, and provide insight into the physical phenomena occurring in the experimental system under bias. Using this analysis, we have modeled the changes in the surface charge density, surface damping, and penetration depth of the resultant modified dielectric function, as well as changes in the index of refraction of the surrounding electrolyte medium. Our approach allowed us to vary these parameters independently but also to understand the result of the effects acting in parallel. We find that the changes in surface damping and charge density play the largest role in modifying the optical response of AuNPs under applied bias, with a smaller dependence on changes induced in the surrounding electrolyte. Based on our analysis we can relate the applied bias to changes in charge density in the AuNPs; the most non-neutral charge state of the shell, a decrease of electron density by 2% compared to bulk, occurred at +2.25 V applied bias and corresponds to roughly 12000 holes in the particle shell (calculated assuming a 2% change of charge density in a 3 nm thick shell of a 30 nm radius Au nanosphere). This analysis is useful as a guide to understanding optical properties of plasmonic nanostructures in non-neutral states or for which the surrounding electrochemical environment is dynamically modified, for example, due to changes of solvent, ion concentration, or photochemical changes. Thus, the results presented here allow us to assess the relative importance of interface damping, surface charging, and index changes on optical extinction of plasmonic nanostructures spanning a large range of conditions relevant for chemical and biological applications.

■ ASSOCIATED CONTENT

Supporting Information

Detailed description of the electrochemical cell fabrication, experimental setup and procedures, simulation and optimization methods, and discussion and figures pertaining to the raw data and fits over the entire measured wavelength range. We have also included the ITO optical data used in simulations. This material is available free of charge via the Internet at http://pubs.acs.org.

■ AUTHOR INFORMATION

Corresponding Author

*E-mail: haa@caltech.edu.

Notes

The authors declare no competing financial interest.

■ ACKNOWLEDGMENTS

The authors gratefully acknowledge support from the Department of Energy, Office of Science under Grant DE-FG02-07ER46405 (M.T.S. and H.A.A.) and for facilities of the DOE "Light-Material Interactions in Energy Conversion" Energy

DOI: 10.1021/ph500358q
ACS Photonics 2015, 2, 459−464

Frontier Research Center (DE-SC0001293). A.M.B. acknowledges support from an NSF Graduate Research Fellowship. Helpful discussions with L. Sweatlock are gratefully acknowledged.

REFERENCES

(1) Atwater, H. A.; Polman, A. Plasmonics for Improved Photovoltaic Devices. *Nat. Mater.* **2010**, *9*, 205−213.
(2) Maier, S. *Plasmonics: Fundamentals and Applications*; Springer: New York, 2007.
(3) Linic, S.; Christopher, P.; Ingram, D. B. Plasmonic-Metal Nanostructures for Efficient Conversion of Solar to Chemical Energy. *Nat. Mater.* **2011**, *10*, 911−21.
(4) Singh Sekhon, J.; S Verma, S. Refractive Index Sensitivity Analysis of Ag, Au, and Cu Nanoparticles. *Plasmonics* **2011**, *6*, 311−317.
(5) Campion, A.; Kambhampati, P. Surface-Enhanced Raman Scattering. *Chem. Soc. Rev.* **1998**, *27*, 241−250.
(6) Miyazaki, T.; Hawegawa, R.; Yamaguchi, H.; Oh-oka, H.; Nagato, H.; Amemiya, I.; Uchikoga, S. Electrical Control of Plasmon Resonance of Gold Nanoparticles Using Electrochemical Oxidation. *J. Phys. Chem. C* **2009**, *113*, 8484−8490.
(7) Persson, B. N. J. Polarizability of Small Spherical Metal Particles: Influence of the Matrix Environment. *Surf. Sci.* **1993**, *281*, 153−162.
(8) Dondapati, S. K.; Ludemann, M.; Muller, R.; Schwieger, S.; Schwemer, A.; Handel, B.; Kwiatkowski, D.; Djiango, M.; Runge, E.; Klar, T. A. Voltage-Induced Adsorbate Damping of Single Gold Nanorod Plasmons in Aqueous Solution. *Nano Lett.* **2012**, *12*, 1247−52.
(9) Mayer, K. M.; Hafner, J. H. Localized Surface Plasmon Resonance Sensors. *Chem. Rev.* **2011**, *111*, 3828−57.
(10) Sannomiya, T.; Dermutz, H.; Hafner, C.; Voros, J.; Dahlin, A. B. Electrochemistry on a Localized Surface Plasmon Resonance Sensor. *Langmuir* **2010**, *26*, 7619−7626.
(11) Novo, C.; Funston, A. M.; Mulvaney, P. Direct Observation of Chemical Reactions on Single Gold Nanocrystals Using Surface Plasmon Spectroscopy. *Nat. Nanotechnol.* **2008**, *3*, 598−602.
(12) Mulvaney, P. Surface Plasmon Spectroscopy of Nanosized Metal Particles Mulvaney. *Langmuir* **1996**, *12*, 788−800.
(13) Kreibig, U.; Vollmer, M. *Optical Properties of Metal Clusters*; Springer: Heidelberg, Germany, 1995.
(14) Malinsky, M. D.; Kelly, K. L.; Schatz, G. C.; Duyne, R. P. V. Nanosphere Lithography: Effect of Substrate on the Localized Surface Plasmon Resonance Spectrum of Silver Nanoparticles. *J. Phys. Chem. B* **2001**, *195*, 2243−2350.
(15) Hilger, A.; Cuppers, N.; Tenfelde, M.; Kreibig, U. Surface and Interface Effects in the Optical Properties of Silver Nanoparticles. *Eur. Phys. J. D* **2000**, *10*, 115−118.
(16) Dahlin, A. B.; Dielacher, B.; Rajendran, P.; Sugihara, K.; Sannomiya, T.; Zenobi-Wong, M.; Voros, J. Electrochemical Plasmonic Sensors. *Anal. Bioanal. Chem.* **2012**, *402*, 1773−84.
(17) Ung, T.; Giersig, M.; Dunstan, D.; Mulvaney, P. Spectroelectrocheistory Of Ag Colloids. *Langmuir* **1997**, *13*, 1773−1782.
(18) Novo, C.; Funston, A. M.; Gooding, A. K.; Mulvaney, P. Electrochemical Charging of Single Gold Nanorods. *J. Am. Chem. Soc.* **2009**, *131*, 14664−6.
(19) Dahlin, A. B.; Sannomiya, T.; Zahn, R.; Sotiriou, G. A.; Voros, J. Electrochemical Crystallization of Plasmonic Nanostructures. *Nano Lett.* **2011**, *11*, 1337−43.
(20) Loo, B. H. In Situ Identification of Halide Complexes on Gold Electrode by Surface-Enhanced Raman Spectrocopy. *J. Phys. Chem.* **1982**, *85*, 433−437.
(21) Müller, J.; Sönnichsen, C.; von Poschinger, H.; von Plessen, G.; Klar, T. A.; Feldmann, J. Electrically Controlled Light Scattering with Single Metal Nanoparticles. *Appl. Phys. Lett.* **2002**, *81*, 171.
(22) Bohren, C. F.; Huffman, D. R. *Absorption and Scattering of Light by Small Particles*; Wiley: New York, 1983.
(23) Dahlin, A. B.; Zahn, R.; Voros, J. Nanoplasmonic Sensing of Metal-Halide Complex Formation and the Electric Double Layer Capacitor. *Nanoscale* **2012**, *4*, 2339−51.
(24) Jing, C.; Rawson, F. J.; Zhou, H.; Shi, X.; Li, W. H.; Li, D. W.; Long, Y. T. New Insights into Electrocatalysis Based on Plasmon Resonance for the Real-Time Monitoring of Catalytic Events on Single Gold Nanorods. *Anal. Chem.* **2014**, *86*, 5513−8.
(25) Hartland, G. V. Optical Studies of Dynamics in Noble Metal Nanostructures. *Chem. Rev.* **2011**, *111*, 3858−87.
(26) Byers, C. P.; Hoener, B. S.; Chang, W. S.; Yorulmaz, M.; Link, S.; Landes, C. F. Single-Particle Spectroscopy Reveals Heterogeneity in Electrochemical Tuning of the Localized Surface Plasmon. *J. Phys. Chem. B* **2014**, *118*, 14047−14055.
(27) Brendel, R.; Bormann, D. An Infrared Dielectric Function Model for Amorphous Solids. *J. Appl. Phys.* **1992**, *71*, 1.
(28) Rakic, A. D.; Djurisic, A. B.; Elazar, J. M.; Majewski, M. L. Optical Properties of Metallic FIlms for Vertical-Cavity Optoelectronic Devices. *Appl. Opt.* **1998**, *37*, 5271−5283.
(29) Lioubimov, V.; Kolomenskii, A.; Mershin, A.; Nanopoulos, D. V.; Schuessler, H. A. Effect of Varying Electric Potential on Surface-Plasmon Resonance Sensing. *Appl. Opt.* **2004**, *43*, 3426−3432.
(30) Templeton, A. C.; Pietron, J. J.; Murray, R. W.; Mulvaney, P. Solvent Refractive Index and Core Charge Influences on the Surface Plasmon Absorbance of Alkanethiolate Monolayer-Protected Gold Clusters. *J. Phys. Chem. B* **2000**, *104*, 564−570.
(31) Pinchuk, A.; Kreibig, U.; Hilger, A. Optical Properties of Metallic Nanoparticles: Influence of Interface Effects and Interband Transitions. *Surf. Sci.* **2004**, *557*, 269−280.
(32) Hendrich, C.; Bosbach, J.; Stietz, F.; Hubenthal, F.; Vartanyan, T.; Trager, F. Chemical Interface Damping of Surface Plasmon Excitation in Metal Nanoparticles: A Study by Persistent Spectral Hole Burning. *Appl. Phys. B: Lasers Opt.* **2003**, *76*, 869−875.
(33) Hövel, H.; Fritz, S.; Hilger, A.; Kreibig, U.; Vollmer, M. Width of Cluster Plasmon Resonances: Bulk Dielectric Functions and Chemical Interface Damping. *Phys. Rev. B* **1993**, *48*, 18178−18188.
(34) Hubenthal, F. Ultrafast Dephasing Time of Localized Surface Plasmon Polariton Resonance and the Involved Damping Mechanisms in Colloidal Gold Nanoparticles. *Prog. Surf. Sci.* **2007**, *82*, 378−387.
(35) Mulvaney, P.; Pérez-Juste, J.; Giersig, M.; Liz-Marzán, L. M.; Pecharromán, C. Drastic Surface Plasmon Mode Shifts in Gold Nanorods Due to Electron Charging. *Plasmonics* **2006**, *1*, 61−66.
(36) Lermé, J.; Baida, H.; Bonnet, C.; Broyer, M.; Cottancin, E.; Crut, A. l.; Maioli, P.; Del Fatti, N.; Vallée, F.; Pellarin, M. Size Dependence of the Surface Plasmon Resonance Damping in Metal Nanospheres. *J. Phys. Chem. Lett.* **2010**, *1*, 2922−2928.
(37) Liebsch, A. Prediction of a Ag Multipole Surface. *Phys. Rev. B* **1998**, *57*, 3803−3806.

DOI: 10.1021/ph500358q
ACS Photonics 2015, 2, 459−464